JOURNAL OF CATALYSIS 104, 86–98 (1987)

Interaction of Nickel Ions with a γ-Al_2O_3 Support during Deposition from Aqueous Solution

P. K. DE BOKX,[1] W. B. A. WASSENBERG, AND J. W. GEUS[2]

Department of Inorganic Chemistry, State University of Utrecht, Croesestraat 77A, 3522 AD Utrecht, The Netherlands

Received December 21, 1984; revised September 22, 1986

The interaction of nickel ions with a γ-Al_2O_3 support was studied using potentiometric titration during deposition from aqueous solution and temperature-programmed reduction of calcined samples. It was found that in calcined samples of low nickel content, nickel is present exclusively as a "surface aluminate." With higher metal loadings a separate NiO phase was detected. From potentiometric titration experiments it was concluded that a precursor of the surface spinel, viz., a mixed hydroxide surface compound, is already formed in aqueous solution. The initial interaction of nickel ions with the alumina support is discussed in terms of specific adsorption of divalent metal ions.

INTRODUCTION

Thermal stability of supported catalysts calls for a strong interaction between the active material and the support. In coprecipitated catalysts this interaction is realized during the precipitation process, which assures an intimate mixing of ions of the support and of the active phase. Coprecipitated catalysts, however, suffer from the serious drawback that the pore structure is formed during thermal treatment of the catalyst, thus making control of the pore structure virtually impossible (*1*). In this paper we will report on support interactions in Ni/γ-Al_2O_3 catalysts prepared by using a well-defined γ-Al_2O_3 (Degussa C) as the support material.

The interaction of nickel ions with an alumina support has been studied using a number of techniques including magnetic measurements (*2–5*), diffuse reflectance spectroscopy (*3–5*), ESCA (*6*), ion scattering spectroscopy (*6*), and temperature-programmed reduction (*7, 8*). The above studies all pertain to impregnated catalysts in their oxidized state. From these investigations it emerged that nickel ions interact strongly with the alumina support, leading to the formation of a "surface" nickel aluminate. The distribution of nickel ions among the octahedral and tetrahedral holes of the spinel was found to be a function of the nickel content, the tetrahedral holes being preferentially occupied at low loadings. At high metal contents (>15 wt%) a separate nickel oxide phase was detected. The formation of the surface spinel and the segregation of the nickel oxide phase was thought to take place during thermal treatment (873 K) of the catalyst samples (*3, 5, 9*). Puxley *et al.* (*9*) arrived at the conclusion that a phase separation between solids containing ions of the support on the one hand, and of the deposited active phase on the other, is a general characteristic of impregnated catalysts. According to these authors only a limited amount of mixed oxide may be formed by calcination.

We have undertaken this study to gain improved insight into the interactions between metal ions and oxidic supports during adsorption/impregnation. Evidence will be provided that mixing of the ions of the active phase and of the support does take

[1] Present address: Philips Research Laboratorium, P.O. Box 80000, 5600 JA Eindhoven, The Netherlands.

[2] To whom all correspondence should be addressed.

0021-9517/87 $3.00

place during the preparation step in aqueous solution due to adsorption of nickel ions onto the support and formation of a mixed hydroxide surface compound. The latter will be shown to be the precursor of the surface nickel aluminate.

To differentiate between processes occurring in aqueous solution and processes taking place during high-temperature calcination, relevant measurements in the aqueous phase have to be made in conjunction with measurements on calcined samples. We have therefore made use of potentiometric titration during deposition from aqueous solution. This technique has found wide acceptance in colloidal and geochemistry (*10–12*), but, in spite of its great merits, it seems to have been only scantily applied in the field of catalyst preparation. Calcined samples have been subjected to temperature-programmed reduction (TPR). Information on the structure and morphology of the catalysts was obtained using X-ray diffraction (XRD) and electron microscopic techniques after both the drying and calcining steps.

EXPERIMENTAL

Apparatus. The potentiometric titration experiments were carried out in a double-walled Pyrex glass vessel (volume 1 liter). The temperature of the solution was controlled by recirculating the water of a water bath between the walls of the vessel. An alkaline solution was introduced below the surface of the solution by means of a Teflon capillary. The rate of the alkali injection was kept at 2.86 μmol/s using a peristaltic pump (Gilson Minipuls II). The pH was continuously measured using an Ingold combi electrode and a Philips PR 9403 mV–pH meter. The electrode was calibrated at the start of each experiment using Electrofact buffer solutions (pH = 4.0 and pH = 7.0 at 293 K). Vigorous stirring and the special design of the vessel eliminated local inhomogeneities as much as possible. Details on the experimental set-up and on its performance can be found elsewhere (*13*). By varying the rate of alkali injection its influence on the results was checked. It was verified that a twofold increase of the aforementioned injection rate did not cause measurable differences in the titration curves. We thus assumed equilibrium to be established during our titration experiments.

TPR experiments were conducted in a combined vacuum/flow apparatus. Samples could be evacuated to base pressures of typically 10^{-4} Pa in a conventional Pyrex high-vacuum system. TPR was carried out in a 10 vol% H_2/Ar flow. The temperature of a cylindrical (i.d. 10 mm) quartz microreactor could be raised linearly using a Eurotherm (type TCS) temperature programmer/controller. The hydrogen consumption was continuously monitored using a thermal conductivity detector kept at a constant temperature of 308 K. Water vapor evolved during reduction was removed using a dry ice/acetone cold trap.

X-ray diffraction (Cu$K\alpha_{1,2}$ radiation) was carried out using either a Debye–Scherrer camera in combination with a microdensitometer (Jenoptik MD 100) or in some cases a Philips PW 1050 diffractometer. Electron microscopy and electron diffraction were performed using Jeol 200 C or Philips 420 electron microscopes. The samples were ultrasonically treated in ethanol. Slurries were applied onto holey carbon films where the ethanol was allowed to evaporate. Nickel contents were measured using a Wilten 351 atomic absorption spectrometer. N_2–BET surface areas and pore size distributions were obtained using a Carlo–Erba Sorptomatic Series 1800.

Materials. A nonporous γ-Al_2O_3 was kindly supplied by the Degussa Corp. (Degussa C). The BET surface area was measured to be 104 m^2/g, in good agreement with the manufacturer's data (*14*). The absence of capillary condensation indicated that the alumina did not contain pores under 200 nm (radius). All chemicals used were of analytical grade. CO_2-free dimineralized water was used in all experiments. Purified sodium hydroxide solutions were standardized against potassium hydrogen phthalate. All potentiometric titra-

tion experiments were carried out under nitrogen to prevent interference of carbonate ions. Most experiments reported here were performed using nickel chloride. The use of nickel nitrate did not induce measurable differences.

Gases used in TPR experiments were technical-grade gases purchased from Hoek-Loos n.v. Hydrogen and argon were purified using successive columns containing a deoxo-catalyst (BASF R-3-11) and a molecular sieve (Linde 4 Å). Oxygen used for calcination was of high quality and used without further purification.

Experimental procedure. A nickel chloride solution (600 ml, 0.1 *M*) was introduced into the double-walled vessel. The pH of the solution was adjusted to 4.0 and the temperature was set to the desired value. It was found that an initial pH lower than 4.0 gave rise to dissolution of the γ-Al_2O_3. An amount of γ-Al_2O_3, corresponding to the intended metal loading, was then added to the solution. After stabilization of the pH the injection of alkali (NaOH, 0.78 *M*) was started. At the end of the experiment (ca. 50 ks) the injection was stopped and the precipitate was filtered off and washed with demineralized water. The precipitate was dried overnight in an oven at 393 K. X-ray diffraction and electron microscopy were employed to characterize the dried catalyst. The catalyst was then pressed (150 MPa), crushed, and sieved to obtain pellets of size range 0.15–0.30 mm (diameter). Typically 100 mg of the pelleted catalyst were introduced into the vacuum system and evacuated to a pressure of 3×10^{-4} Pa. The sample was calcined at a heating rate of 0.083 K/s in 3 kPa oxygen to a temperature of 750 K. The sample was held at this temperature for an hour. Prolonging the calcination time to 2 h did not cause obvious differences in subsequent reduction behavior. The sample was cooled to room temperature and pumped to 3×10^{-4} Pa. For investigation with TPR a flow of 10% H_2/Ar at a total flow rate of 0.33 ml/s was passed through the sample. The linear heating rate used in all experiments was 0.145 K/s. Samples calcined according to an identical schedule were investigated using XRD and electron microscopy.

In some cases nickel contents of samples taken in the early stages of preparation were determined using atomic absorption spectroscopy (AAS). During the titration 25-ml samples were taken with a pipet at predetermined intervals. The samples were filtered, washed, and dried as described above. Sample destruction was performed according to a procedure closely analogous to the one described by Juette *et al.* (*15*). Sample solutions were diluted to obtain concentrations between 1 and 10 mg/liter. The AAS measurements were carried out in an acetylene/air flame at a wavelength of 232 nm.

RESULTS

Potentiometric Titration

Titration experiments were performed at temperatures of 277, 298, 315, and 362 K. A typical set of titration curves, pH versus OH/Ni ratio, is shown in Fig. 1. Metal loadings (wt%, defined as the weight ratio [nickel/(nickel + Al_2O_3)] $\times$ 100%) are indicated in the figure. The curve designated $Ni(OH)_2$ refers to the precipitation of nickel hydroxide in the absence of the support. From the height of the plateau and the known nickel concentration the solubility product of nickel hydroxide can be evaluated. The value obtained at 298 K ($K_{sp} = 10^{-15.6}$) lies well within the range reported previously (*16*). It can be seen that initially all curves recorded with suspended alumina deviate from the $Ni(OH)_2$ curve. It is evident that nickel ions are consumed in a process not leading to nickel hydroxide, as the solubility product of $Ni(OH)_2$ is not reached here. At high nickel contents the curves coincide with the $Ni(OH)_2$ curve from the points marked by arrows in Fig. 1. With increasing metal loadings these points of coincidence move to smaller OH/Ni values. Clearly, in these catalysts nickel hydroxide is also formed. The amount of nickel hydroxide in these samples can be calculated from the amount of alkali con-

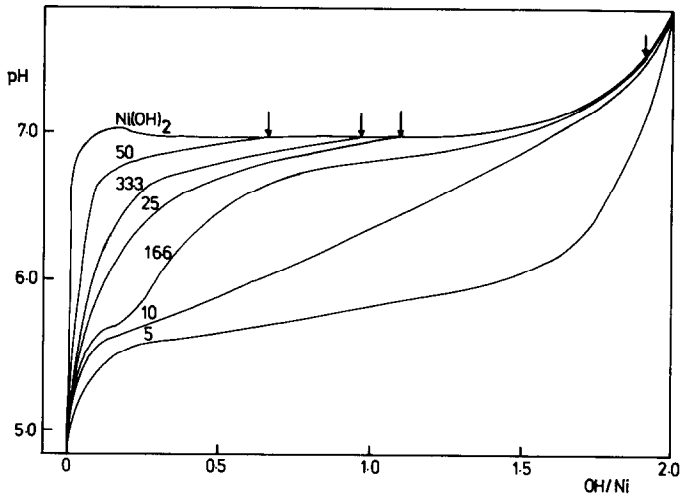

FIG. 1. Titration curves for various metal loadings obtained with alkali injection at 315 K. Injection rate: 2.68 μmol NaOH/s; initial nickel chloride concentration: 0.1 *M*. Arrows indicate points of coincidence with the curve of unsupported $Ni(OH)_2$.

sumed from the points of coincidence to the endpoints of the titration (the point of inflection in the final steep pH increase). It should be noticed that although a "compound" different from nickel hydroxide is formed initially, the OH/Ni stoichiometry of this compound is almost equal to 2 as is evidenced from the fact that all titration curves have their endpoints at OH/Ni ratios of about 2. The amount of nickel deposited in a form different from nickel hydroxide can thus be calculated from the amount of alkali consumed from the start of the titration up to the point of coincidence with the $Ni(OH)_2$ curve.

Although all samples with metal loadings lower than about 13 wt% contain negligible amounts of nickel hydroxide, only the lowest metal loading shows a plateau characteristic of the occurrence of a single process. This initial interaction of nickel ions with an alumina support has been investigated further and the results are presented in Fig. 2. Here the amount of nickel taken up by the alumina (adsorbed) is plotted as a function of pH. The figure includes data points derived from titration curves (triangles) assuming an OH/Ni stoichiometry of 2 for the adsorption process. Also indicated in Fig. 2 are the adsorbed amounts determined by AAS. The highest point corresponds to a metal loading of about 2.5 wt%. The solid curve is a fit based on a coordinative adsorption model (see Discussion).

Finally, it was observed that the samples of a low nickel content had a light blue color, whereas those of high nickel content exhibited the typical green color of nickel hydroxide.

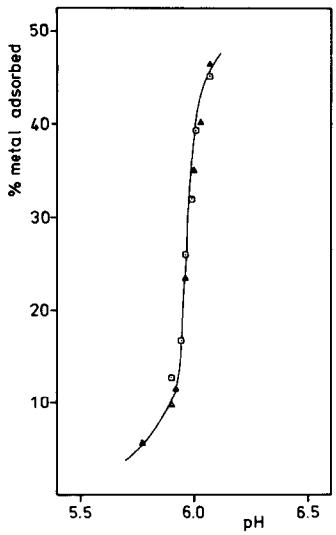

FIG. 2. The pH dependence of adsorption of Ni^{2+} ions onto γ-Al_2O_3 at 298 K (initial nickel concentration: 0.1 *M*, 92.5 g Al_2O_3/dm^3).

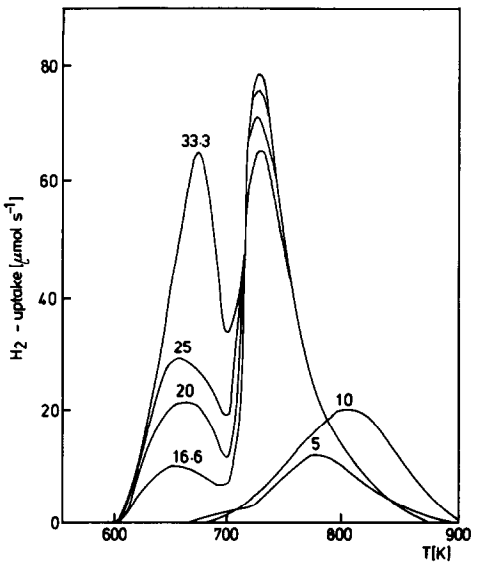

FIG. 3. TPR profiles of catalysts prepared at 315 K (flow: 0.33 ml/s 10% H_2/Ar, heating rate: 0.145 K/s).

Temperature-Programmed Reduction

In Fig. 3 the TPR profiles of the calcined samples are shown. Again the numbers indicate the nickel loadings. At low loadings one high temperature (800 K) reduction peak is observed. At higher loadings a two-peak reduction pattern is displayed. This pattern is very similar to results obtained previously (*7, 8*). The reported peak maxima show some scatter, however, most probably due to differences in the employed calcination procedure. As was done by Zielinski (*7*), the low-temperature peak was attributed to NiO reduction by comparison with the reduction behavior of a physical NiO/γ-Al_2O_3 mixture. The above author ascribed the high-temperature peak to the reduction of nickel that had reacted with the alumina to a presumably nonstoichiometric nickel aluminate. The latter will be referred to as "fixed nickel" in the following, as opposed to "free nickel" (NiO).

It can be seen that the high-temperature peak shifts to lower temperatures when nickel oxide is present in the samples. We attribute this temperature shift to the catalytic effect of metallic nickel on the reduction of the nickel aluminate. Arnoldy and Moulijn (*17*) observed similar shifts studying the Co/γ-Al_2O_3 system, which is closely related to the system considered here (*2*). However, the influence of an intrinsic effect on reducibility due to the well-established fact that nickel in tetrahedral holes is more difficult to reduce than nickel in octahedral holes cannot be excluded.

The TPR profiles were deconvoluted assuming symmetrical peaks. The results are presented in Fig. 4: Both the amounts of nickel found as free nickel and as fixed nickel are shown as a function of the total nickel content. Open squares represent the results of the TPR measurements. Also indicated (full squares) are the amounts of free nickel ($Ni(OH)_2$) and fixed nickel calculated from the titration curves as elaborated in the previous paragraph. The good agreement between the results obtained in aqueous solution and by TPR of calcined samples is evident. The amounts of nickel deposited as fixed nickel are collected in Table 1 as a function of the preparation temperature. It is seen that this amount decreases with increasing temperature. It also follows from Table 1 that quantities determined with potentiometric titration are invariably slightly higher than the TPR results. A possible explanation for this discrepancy can be found in the employed deconvolution procedure which is not without ambiguity.

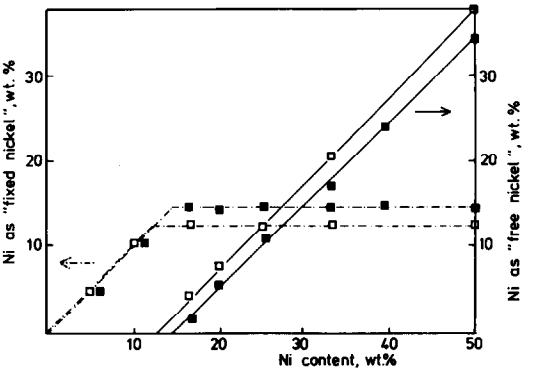

FIG. 4. Composition of catalyst samples prepared at 315 K (open squares; TPD data; full squares: potentiometric titration data).

TABLE 1

Amounts of Nickel Deposited as Fixed Nickel as a Function of the Preparation Temperature

T (K)	By TPR (μmol/m^2)	By potentiometric titration (μmol/m^2)
277	33.5	38.5
298	24.9	29.9
315	23.6	27.2
361	15.1	16.4

Note. Estimated relative errors: 5%.

Structure of the Catalysts

X-ray diffractograms of dried uncalcined catalysts have been collected in Fig. 5. As expected from the potentiometric titration results, reflections due to $Ni(OH)_2$ lines are totally absent in the pattern of the 10 wt% catalyst. They can clearly be seen in that of the 50 wt% sample. With both catalysts new reflections due to d spacings of 0.78, 0.39, and 0.257 nm are present. These lines can be ascribed to the Ni/Al member of a group of compounds generally known as Feitknecht compounds (*9*). These compounds have the general formula:

$$Me_x^{2+}Me_y^{3+}(OH^-)_{2x+3y-2z}A_z^{2-} \cdot nH_2O,$$

where $Me^{2+} = Mg^{2+}$, Mn^{2+}, Fe^{2+}, Co^{2+}, Ni^{2+}, Cu^{2+}, Zn^{2+}, etc.;
$Me^{3+} = Al^{3+}$, Fe^{3+}, Cr^{3+}, etc.;
$A^{2-} = CO_3^{2-}$, SO_4^{2-}, or twice as many NO_3^-, OH^-, Cl^-, Br^-.

The Ni/Al member occurs naturally as the mineral takovite (*18*). According to Allmann (*19*), the structure should be described in terms of brucite-like layers in which some of the divalent metal ions have been replaced by trivalent ones. The excess charge is compensated by an interlayer of anions. This interlayer also contains water. The distance between adjacent brucite layers is around 0.78 nm. The indexing of the X-ray pattern depends on the stacking of the brucite layers, leading to either rhombohedral or hexagonal order. From the

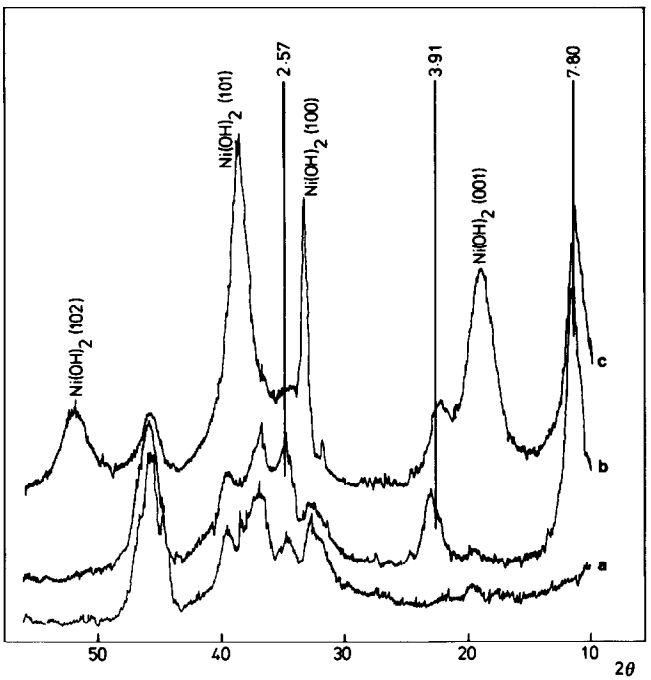

FIG. 5. X-ray diffractograms of dried, uncalcined catalysts prepared at 315 K. (a) pattern of the γ-Al_2O_3 support, (b) pattern of a 10 wt% catalyst, (c) pattern of a 50 wt% catalyst (d spacings in Å are indicated).

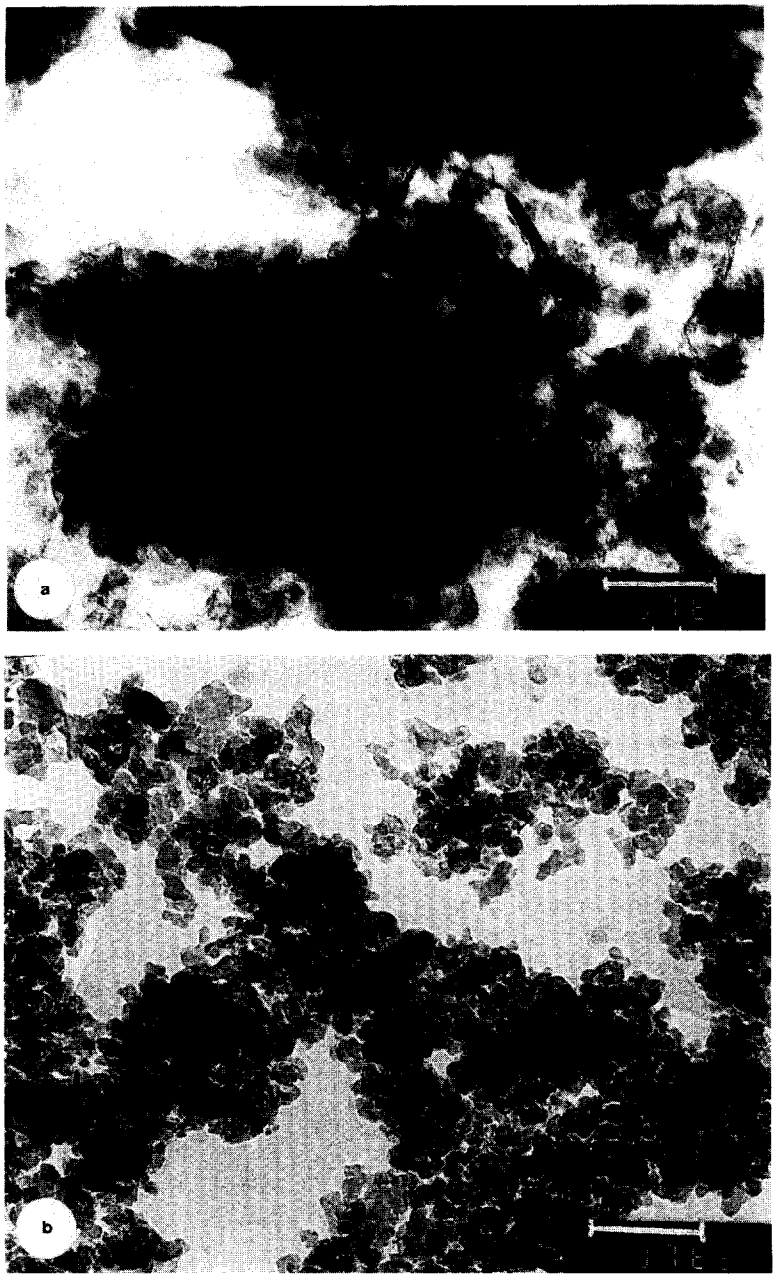

FIG. 6. (a) Electron micrograph of a 50 wt% catalyst prepared at 315 K, showing needle- and plate-like structures. (b) Electron micrograph of a 10 wt% catalyst prepared at 315 K. Bars in the right-hand corners indicate 100 nm.

present data this information can obviously not be derived. However, the observed lines are most probably due to inter-brucite layer reflections, for example the (003l), l = 1, 2, 3 reflections of the rhombohedral cell. As the chemical composition of the Ni/Al mixed hydroxide (notably the identity of the anions in the interlayer) is not known, it will be referred to generally as the Feitknecht compound in the following.

In Fig. 6a an electron micrograph of a 50 wt% catalyst is shown. Notice the needle-

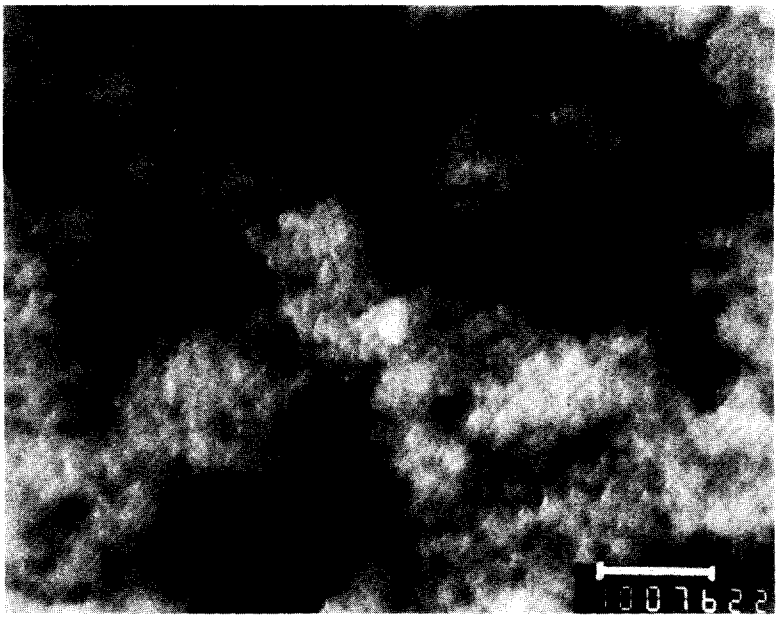

FIG. 7. Dark-field image of a 10 wt% catalyst prepared at 315 K. Tilt angle corresponds to the 0.78-nm reflection. The bar in the right-hand corner indicates 100 nm.

and plate-like structures. The plate-like structures are totally absent in the 10 wt% catalyst (Fig. 6b). As both nickel hydroxide and the Feitknecht compounds, due to their sandwich-like lattices, are known to give rise to shape anisotropy, the absence of platelets and needles was somewhat surprising at first. To determine where the Feitknecht compound was located use was made of the dark-field technique. Here the image is not formed by transmitted electrons but, in tilting the incident beam, by electrons which satisfy distinct diffraction conditions. In Fig. 7a dark field image, using a tilt angle corresponding to the 0.78-nm reflection, is shown. As large parts of the alumina surface are contrasted, a close contact between the alumina and the Feitknecht phase is suggested. Another indication for strong interaction between the Feitknecht phase and the alumina support can be obtained from ion-exchange studies. Feitknecht compounds are known to exchange incorporated anions really, accompanied by changes in brucite layer spacing (*20*). It was found that leaving a 10 wt% catalyst sample in a 0.1 *M* sodium sulfate solution at 333 K for over 250 ks did not lead a significant changes in brucite layer spacing. From these observations and from the fact that (*hk*0) reflections are not detected in the X-ray diffractograms, we conclude that the Feitknecht phase is present on the alumina surface in the form of a thin layer.

Calcined samples containing less than 15 wt% Ni did not reveal any diffraction lines due to NiO. These lines could be readily distinguished in the samples of higher nickel content. No significant evidence of the presence of $NiAl_2O_4$ could be derived from X-ray data, in contrast to the results obtained by Lo Jacono *et al.* (*3*). This could possibly be due to the low calcination temperature used in our experiments (750 K versus 873 K (*3*)). The decomposition of the Ni/Al Feitknecht compounds at low temperatures is known to yield very poorly crystallized, defective nickel aluminate (*21*).

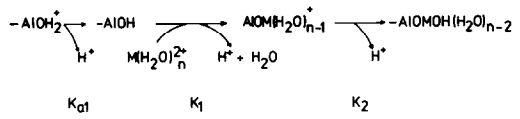

FIG. 8. Representation of the consecutive steps of a coordinative adsorption model (cf. Ref. (*27*))

DISCUSSION

The specific adsorption of divalent metal ions on amphoretic surfaces has received a great deal of attention over the years (*22*). The word "specific" is used here to indicate that adsorption constants differ within a group of cations of the same valency. An obvious implication of this specificity is that not only electrostatic but also coordinative interactions are involved in the adsorption process. A number of models to describe specific adsorption have been proposed (*22–26*). It is generally assumed that the oxide surface consists of a distinct number of hydroxyl groups (sites). The essence of most models is an ion-exchange process in which cations upon adsorption replace bound protons at the surface sites. Models differ inter alia in the treatment of the sequence of events which takes place, for instance, the adsorption of hydrolyzed cations (*25*) versus the surface hydrolysis of adsorbed cations (*26*). No consensus on the details of the adsorption process has been reached as yet.

Very recently a model has been proposed claiming to yield good fits of the experimental data in the concentration range of interest to catalyst preparation (*27*), whereas other models seem to be applicable only at very low metal ion concentrations. We will apply this model to our results. Although details are to be found in the original paper and references therein, a brief outline of the proposed adsorption mechanism will now be given. The double-layer model is represented in Fig. 8, where $AlOH_2^+$ is the protonated surface hydroxyl group; $-AlOM^+(H_2O)_{n-1}$ and $-AlOMOH(H_2O)_{n-2}$ are two kinds of surface complex formed by adsorption of $M(H_2O)_n^{2+}$ and surface hydrolysis of the $-AlOM^+(H_2O)_{n-1}$ species, respectively. K_1 and K_2 are the equilibrium constants for these steps. K_{a_1} is the acidity constant of the surface hydroxyl groups. As K_{a_1} is taken to be independent of coverage, the model is expected to produce good fits for low coverages only. It can be seen from Fig. 8 that this model satisfies the observed OH/Ni stoichiometry of 2.

The intrinsic equilibrium constants can be related to measurable quantities (adsorbed amounts, bulk concentrations and surface potential) according to

$$K_1^{\text{int}} \frac{\exp(e\psi_s/kT)}{[H^+]} + K_1^{\text{int}} K_2^{\text{int}} \left\{\frac{\exp(e\psi_s/kT)}{[H^+]}\right\}^2 = \frac{[M^{2+}]_{\text{ad}} \exp(2e\psi_s/kT)}{[-AlOH][M(H_2O)_n^{2+}]}. \quad (1)$$

For a derivation of this expression and description of the symbols the reader is referred to the Appendix. The amounts adsorbed as a function of pH were determined experimentally as described in the previous paragraph (Fig. 2). Thus, if the intrinsic acidity constant of alumina, the total number of surface sites, and the surface potential as a function of pH are known, K_1^{int} and K_2^{int} can be evaluated. The intrinsic acidity constants was taken to be 1.585×10^{-7} according to Ref. (*27*), and the total number of surface sites 1.3×10^{21}/g γ-Al_2O_3 from our measurement of the surface area and the assumption of 12.5 OH^-/nm^2 (*28*). The surface potential is more difficult to establish as specific adsorption obviously induces deviations from a behavior according to the Nernst law. From results of Co^{2+} adsorption we estimated ψ_s to be 75 mV at pH = 6.0 and to be independent of pH in the narrow pH range under consideration. Results of the fitting procedure are shown in Figs. 9 and 10. In Fig. 9 it is shown that the parabolic relation dictated by Eq. (1) is indeed obeyed. From the coefficients of the quadratic equation the equilibrium constants can thus be obtained. After Hachiya

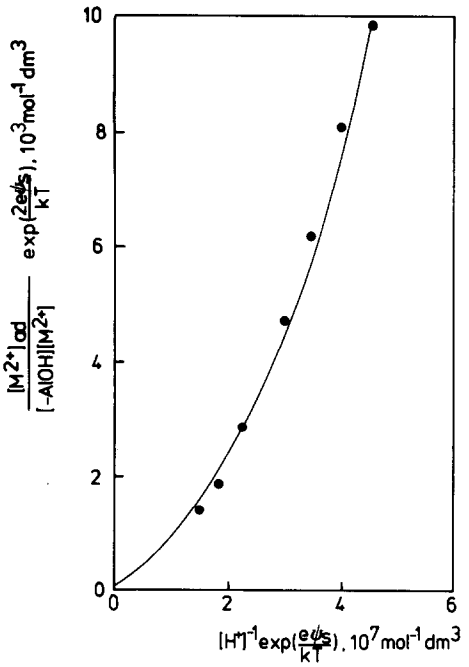

FIG. 9. Plot of $\{[M^{2+}]_{ad}/([AlOH][M(H_2O)_n^{2+}])\}$ $\exp(2e\psi_s/kT)$ versus $[H^+]^{-1}\exp(e\psi_s/kT)$.

et al. (*27*) the equilibrium constants have been plotted as a function of the first hydrolysis of the metal ion (*29*). Our values for nickel adsorption ($pK_1^{int} = 4.0 \pm 0.2$ and $pK_2^{int} = 7.4 \pm 0.2$) have been supplemented to their Figure (Fig. 10). As can be seen from Fig. 10 a fair correlation with the hydrolysis constant is obtained. It is noteworthy to mention here that an error of 25 mV in the surface potential gives rise to changes in pK_1^{int} and pK_2^{int} values of about 0.3.

Notwithstanding the admittedly rather crude estimation of the surface potential, valuable insight can be gained from the above approach, viz., the decisive importance of pH during adsorption/impregnation. As has been pointed out by Acres *et al.* (*30*), the pH is seldomly measured in catalyst preparation studies and its influence is very often overlooked. With the aid of the data collected in Fig. 10 the extent of adsorption of different cations at given pH values can now be estimated. For example, the adsorption of Co^{2+} ions onto γ-Al_2O_3 at pH = 3 is shown to be completely negligible. Thus, one would not expect to obtain highly dispersed catalysts under these conditions, as corroborated by the experiments reported by van 't Blik (*31*).

We now turn to the maximum amount of nickel that is taken up by the alumina. As has been stated in the above, models describing metal ion take-up quantitatively fail at high coverages, because one of the premises, viz., homogeneity of surface sites, is not correct. Indeed, the heterogeneity of the surface, and possibly even multilayer adsorption, should be taken into consideration at high adsorption densities. The heterogeneity of the surface, i.e., a gradual change of the acidity constants of the hydroxyl groups, is reflected in the form of the titration curves. A smooth pH increase, indicative of, for example, a coverage-dependent acidity constant, is observed at high metal loadings. As no models seem to be available for high adsorption densities, we will discuss our results on a qualitative basis. In Table 2 the amounts deposited as fixed nickel have been tabulated. The good agreement between the various experimental techniques is apparent. Especially, the good agreement between our potentiometric results and results obtained on calcined samples deserves further attention, strongly suggesting that a precursor of the surface spinel is

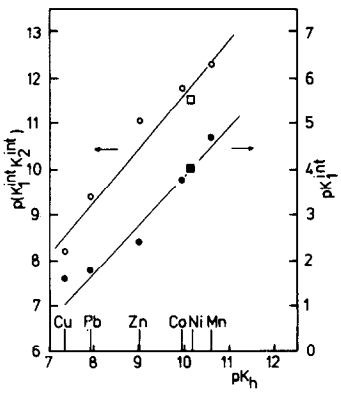

FIG. 10. Logarithmic plot of $K_1^{int}K_2^{int}$ (open symbols) and K_1^{int} versus the hydrolysis constant. Squares denote our results for nickel adsorption.

TABLE 2

Amounts of Nickel Deposited as Fixed Nickel at 298 K: Comparison of results from various techniques

Amount deposited as fixed nickel (μmol/m^2)	Technique	Ref.
34.9	ESCA ISS	(6)
26.6	TPR	(7)
24.9	TPR	This work
29.9	Potentiometric titration	This work

already formed in aqueous solution and not, as has been suggested earlier, by an interdiffusion process during calcination.

We recall that a Feitknecht compound could be detected by diffraction experiments after the drying step. From electron microscopy and ion-exchange studies we concluded that the Feitknecht phase is deposited onto the alumina support in the form of a thin layer. As a consequence of this evidently strong interaction of the Feitknecht phase with the alumina, one would expect distinct epitaxial relations to exist between the two solid phases. From the dark-field experiments we conclude that the basal planes of the Feitknecht compound are perpendicular to the alumina surface. This can be appreciated by realizing that due to the short wavelength of electrons, diffraction can only be observed if the incident beam is almost parallel to the lattice planes. As large parts of the alumina surface are displayed brightly in the dark-field images, the (003*l*) planes of the Feitknecht compound must be perpendicular to the surface. In Fig. 11 a possible epitaxy, in accordance with the above results, is presented. It is assumed that the γ-Al_2O_3 predominantly exposes (100) planes (*32*). In the upper part of the left-hand side of the figure the position of the octahedral holes is depicted, while the lower part shows the adsorption of Ni^{2+} ions onto the γ-Al_2O_3 (100) plane. Aluminum vacancies are denoted by Al*. The growth of the Feitknecht compound on the alumina support is illustrated in the right-hand side of Fig. 11.

The "crystallite size" of the Feitknecht phase was estimated from X-ray line broadenings using the Scherrer equation. Warren's correction for the instrumental line broadening was employed (*33*). From the line broadening of the (003 *l*) reflections, the average dimension along the alumina surface (compare Fig. 11) was estimated to be around 5 nm. The dimension perpendicular to the alumina surface ("layer thickness") is beyond determination as no reflections having nonzero *h* or *k* values were observed. Comparison of the amounts of nickel deposited as Feitknecht compound with the total number of surface sites available yields a nickel ion/surface site ratio of about 1.5. We propose that a Feitknecht compound is formed due to multilayer adsorption of nickel ions with the possible incorporation of aluminum atoms from the alumina. At a very distinct and remarkably reproducible (Table 2) metal loading formation of the Feitknecht phase ceases and a separate nickel hydroxide phase precipitates. We speculate that the Feitknecht phase becomes progressively more difficult to form as coverage increases. At a certain loading the pH level corresponding to the solubility product of nickel hydroxide is reached and $Ni(OH)_2$ is precipitated. How-

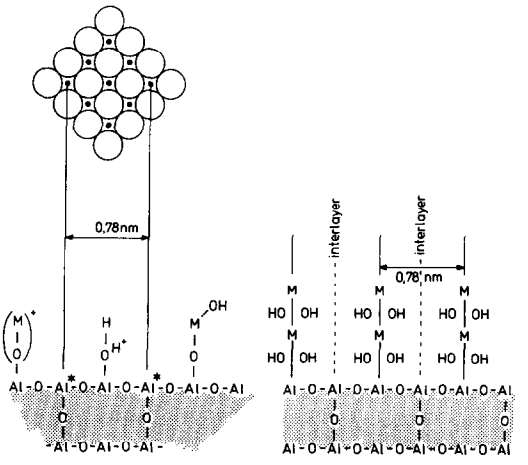

FIG. 11. Adsorption of Ni^{2+} ions and desorption at a Feitknecht compound onto γ-Al_2O_3 (see text).

ever, the question why this occurs at the particular metal loading quoted in Table 2 remains unresolved. Also the interpretation of the temperature dependence of the amount deposited as Feitknecht compound is difficult on the basis of the present data. If our explanation for the occurrence of a distinct coverage of the Feitknecht phase is correct, the observed decrease with temperature (Table 1) is due to a decrease of the stability of the Feitknecht phase relative to nickel hydroxide. Without additional information on the temperature dependence of the stability of clay minerals, like Feitknecht compounds, prediction of deposited amounts, other than by interpolation of empirical data, is not possible.

As a final remark we would like to mention that Feitknecht compounds and related clay minerals seem to be more general than is commonly realized. They have been detected, sometimes unknowingly, in Ni/Al_2O_3 (*9*), Ni/TiO_2 (*34*), Ni/SiO_2 (*35*), and Fe/MgO (*36, 37*) catalysts. Investigations of the way these compounds originate and decompose are of great interest to the study of oxide-supported catalysts.

CONCLUSIONS

(i) Potentiometric titration is a valuable tool for acquiring information on interactions taking place in aqueous solutions.

(ii) The initial interaction between nickel ions and a γ-Al_2O_3 support can be quantitatively described using a coordinative adsorption model.

(iii) The surface nickel aluminate reported by many authors is formed during calcination by decomposition of a mixed hydroxide precursor (Feitknecht compound).

(iv) The amount of Feitknecht compound is limited to a maximum. This maximum amount decreases with increasing temperature of preparation. In samples containing more metal than corresponding to the maximum of the Feitknecht phase a separate nickel hydroxide phase is formed.

APPENDIX

NOMENCLATURE

e	elementary charge
k	Boltzmann constant
K_i	equilibrium constant of step i
K_i^{int}	intrinsic equilibrium constant of step i
$[\mathbf{I}]$	concentration of component **I**
$[\mathbf{I}]_S$	surface concentration of component **I**
ψ_s	surface potential at the plane of adsorption

The equilibrium constants K_1, K_2 and K_{a_1} are defined in the usual way according to

$$K_1 = \frac{[-\mathrm{AlOM(H_2O)}_{n-1}^{+}][\mathrm{H^+}]}{[-\mathrm{AlOH}][\mathrm{M(H_2O)}_n^{2+}]} \qquad \text{(A-1)}$$

$$K_2 = \frac{[-\mathrm{AlOMOH(H_2O)}_{n-2}][\mathrm{H^+}]}{[-\mathrm{AlOM(H_2O)}_{n-1}^{+}]} \qquad \text{(A-2)}$$

$$K_{a_1} = [-\mathrm{AlOH}][\mathrm{H^+}]/[\mathrm{AlOH_2^+}]. \qquad \text{(A-3)}$$

As adsorption on charged surfaces is involved, the concentrations of ionic species at the solid/liquid interface will differ from their concentrations in the bulk liquid phase. Provided M^{2+} and H^+ are adsorbed on the same plane, their bulk concentrations can be related to surface concentrations via similar Boltzmann distributions:

$$[\mathrm{M(H_2O)}_n^{2+}] = [\mathrm{M(H_2O)}_n^{2+}]_s \exp(2e\psi_s/kT) \qquad \text{(A-4)}$$

$$[\mathrm{H^+}] = [\mathrm{H^+}]_s \exp(e\psi_s/kT). \qquad \text{(A-5)}$$

Equilibrium constants can now be rewritten in terms of intrinsic equilibrium constants, i.e., equilibrium constants in the absence of an electric field, by substituting (A-4) and (A-5) in Eqs. (A-1)–(A-3):

$$K_1 = K_1^{int} \exp(-e\psi_s/kT) \qquad \text{(A-6)}$$

$$K_2 = K_2^{int} \exp(e\psi_s/kT) \qquad \text{(A-7)}$$

$$K_{a_1} = K_{a_1}^{int} \exp(e\psi_s/kT). \qquad \text{(A-8)}$$

Using the equalities

$$[\mathrm{M^{2+}}]_{ad} = [-\mathrm{AlOM(H_2O)}_{n-1}^{+}] + [-\mathrm{AlOMOH(H_2O)}_{n-2}] \qquad \text{(A-9)}$$

$$[-\mathrm{AlOH}] = [-\mathrm{AlOH}]_t - [-\mathrm{AlOH}_2^+] - [\mathrm{M}^{2+}]_{ad} \quad \text{(A-10)}$$

$$[-\mathrm{AlOH}_2^+] = \frac{[-\mathrm{AlOH}]_t - [\mathrm{M}^{2+}]_{ad}}{1 + K_{a_1}^{int} \exp(e\psi_s/kT)/[\mathrm{H}^+]} \quad \text{(A-11)}$$

and combining (A-1)–(A-3) and (A-6) and (A-7) leads to

$$K_1^{int} \frac{\exp(e\psi_s/kT)}{[\mathrm{H}^+]} + K_1^{int} K_2^{int} \frac{\exp(e\psi_s/kT)^2}{[\mathrm{H}^+]} = \frac{[\mathrm{M}^{2+}]_{ad} \exp(e\psi_s/kT)}{[-\mathrm{AlOH}][\mathrm{M}(\mathrm{H_2O})_n^{2+}]}. \quad \text{(A-12)}$$

ACKNOWLEDGMENTS

The authors are indebted to Prof. Dr. P. Biloen and Dr. A. J. H. M. Kock for helpful discussions. The experimental assistance of Mr. A. R. Balkenende, Mr. R. L. C. Bonne, and Mr. A. F. H. Wielers is gratefully acknowledged. These investigations were financially supported by the VEG-Gasinstituut n.v.

REFERENCES

1. Geus, J. W., in "Preparation of Catalysts III" (G. Poncelet, P. Grange, and P. A. Jacobs, Eds.), p. 1. Elsevier, Amsterdam, 1983.
2. Rymer, G. T., Bridges, J. M., and Tomlinson, J. R., *J. Phys. Chem.* 65, 2152 (1961).
3. Lo Jacono, M., Schiavello, M., Cimino, A., *J. Phys. Chem.* **75,** 1044 (1971).
4. Cimino, A., Lo Jacono, M., Schiavello, M., *J. Phys. Chem.* **79,** 243 (1975).
5. Lo Jacono, M., Schiavello, M., *in* "Preparation of Catalysts" (B. Delmon, P. A. Jacobs, and G. Poncelet, Eds.), p. 473. Elsevier, Amsterdam, 1976.
6. Wu, M., and Hercules, D. M., *J. Phys. Chem.* **83,** 2003 (1979).
7. Zielinski, J., *J. Catal.* **76,** 157 (1982).
8. Little, J. A., Butler, G., Daish, S. R., and Tumbridge, J. A., *in* "Proceedings, 8th International Congress on Catalysis, Berlin, 1984," Vol. 5, p. 239. Dechema, Frankfurt am Main, 1984.
9. Puxley, D. C., Kitchener, I. J., Komodromos, C., and Parkyns, N. D., *in* "Preparation of Catalysts III" (G. Poncelet, P. Grange, and P. A. Jacobs, Eds.), p. 237. Elsevier, Amsterdam, 1983.
10. Parks, G. A., and de Bruyn, P. L., *J. Phys. Chem.* **66,** 967 (1962).
11. Stol, R. J., Ph.D. thesis. State University of Utrecht, Utrecht, 1978.
12. James, R. O., Stiglich, P. J., and Healy, T. W., *Faraday Disc. Chem. Soc.* **59,** 142 (1975).
13. Vermeulen, A. C., Geus, J. W., Stol, R. J., and de Bruyn, P. L., *J. Colloid Interface Sci.* **51,** 449 (1975).
14. Degussa, Technical Bulletin Pigments, No. 56.
15. Juette, B. A. H., Heikamp, A., and Agterdenbos, J., *Anal. Chem. Acta* **110,** 345 (1979).
16. Feitknecht, W., *Pure Appl. Chem.* **6,** 130 (1963).
17. Arnoldy, P., and Moulijn, J. A., *J. Catal.* **93,** 38 (1985).
18. Maksimovic, Z., *C. R. Seances Serbe Geol.*, 130 (1955).
19. Allmann, R., *Chimia* **24,** 99 (1970).
20. Bish, D. L., *Bull. Mineral.* **103,** 170 (1980).
21. Rikhter, K., Ketchik, S. V., Simonova, L. G., and Borisova, M. S., *Kinet. Catal. (English trans.)* **16,** 1121 (1975).
22. Davis, J. A., James, R. O., and Leckie, J. O., *J. Colloid Interface Sci.* **63,** 480 (1978), and references therein.
23. Yates, D. E., Levine, S., and Healy, T. W., *J. Chem. Soc. Faraday Trans. I* **70,** 1807 (1974).
24. Davis, J. A., and Leckie, J. O., *J. Colloid Interface Sci.* **67,** 196 (1978).
25. James, R. O., and Healy, T. W., *J. Colloid Interface Sci.* **40,** 65 (1972).
26. Huang, C-P., and Stumm, W., *J. Colloid Interface Sci.* **43,** 409 (1973).
27. Hachiya, K., Sasaki, M., Ikeda, T., Mikami, N., and Yasunaga, T., *J. Phys. Chem.* **88,** 23 (1984).
28. Knözinger, H., and Ratnasamy, P., *Catal. Rev. Sci. Eng.* **17,** 31 (1978).
29. Sillén, L. G., Ed., "Stability Constants of Metal-Ion Complexes," Suppl. No. 1, Chem. Soc. London, 1971.
30. Acres, G. J. K., Bird, A. J., Jenkins, J. W., and King, F., *in* "Catalysis," Vol. 4, "A Specialist Periodical Report," p. 1. The Royal Society of Chemistry, London, 1981.
31. van 't Blik, H. F. J., Ph.D. thesis. Technological University, Eindhoven, 1984.
32. Peri, J. B., *J. Phys. Chem.* **70,** 3168 (1966).
33. Klug, M. P., and Alexander, L. E., "X-ray Diffraction Procedures," 2nd ed. Wiley, New York, 1974.
34. Rubinstein, A. M., Dulov, A. A., Slinkin, A. A., Abramova, L. A., Gershenzon, I. Sh., Gorskaya, L. A., Danyushevskii, V. Ja., Dashevskii, M. I., Klyachko-Gurvich, A. L., Lavroskaya, T. K., Lafer, L. I., and Yakerson, V. I., *J. Catal.* **35,** 80 (1974).
35. Hermans, L. A. M., and Geus, J. W., *in* "Preparation of Catalysts II" (B. Delmon, P. Grange, P. Jacobs, and G. Poncelet, Eds.), p. 113. Elsevier, Amsterdam, 1979.
36. Boudart, M., Delbouille, A., Dumesic, J. A., Khammouma, S., and Topsøe, H., *J. Catal.* **37,** 486 (1975).
37. Kock, A. J. H. M., Fortuin, H. M., and Geus, J. W., *J. Catal.* **96,** 261 (1985).